Crystallization of Fiber-Reinforced Poly(phenylene sulfide) Composites. II. Modeling the Crystallization Kinetics

GLENN P. DESIO* AND LUDWIG REBENFELD†

TRI/Princeton, and Department of Chemical Engineering, Princeton University, P.O. Box 625, Princeton, New Jersey 08542

SYNOPSIS

The kinetic data obtained by differential scanning calorimetry for the isothermal crystallization from the melt of unreinforced poly(phenylene sulfide) (PPS) and of model carbon, aramid, and glass fiber-reinforced PPS composites has been analyzed and modeled on the basis of the Avrami equation. The classical Avrami model provided a good description of the volume fraction crystallized for PPS and for those composites that did not exhibit transcrystallinity in thin-film specimens. Nonlinear Avrami behavior was observed for those composite systems that did exhibit transcrystallinity, for which parallel and series dual Avrami models were used. A series crystallinity model, which corrects the volume fraction crystallized for structural imperfections, was applied to all the systems, providing a reasonable modeling of the data. In this model, we postulate an initial primary crystallization followed by a secondary crystallization. The temperature dependencies of the Avrami rate constants were analyzed through Arrhenius relationships, and the resultant activation energies and frequency factors were interpreted in terms of nucleation and growth phenomena. We found the frequency factor for primary crystallization to be indicative of the nucleating abilities of the fiber surfaces and to correlate with the presence of transcrystallinity.

INTRODUCTION

The formation of a crystalline state from a polymer melt involves nucleation of the crystalline phase and growth of the crystal structure. We have previously reported on the experimental aspects of the crystallization kinetics of poly(phenylene sulfide) (PPS) composites.[1,2] Our attention in the earlier papers concentrated on crystallization half-time and degree of crystallinity measurements. In this paper, we turn our attention to the modeling of our data to investigate the mechanisms of nucleation and crystal growth.

We have taken two approaches to the modeling of our data. In the first, we use the Avrami model to analyze the development of the overall volume fraction of crystallized material with time.[3] Recent studies indicate that the Avrami model can, in most cases, be used to describe the crystallization of composites.[4-7] In some composite systems, the Avrami approach yields only partially satisfactory results in that it can be used to model the crystallization process only at short times.[5,8-10] In the second approach, we model the development of crystallinity rather than the volume fraction of material crystallized. We treat the development of crystallinity with time in a manner analogous to the Avrami model.

APPLICATION OF THE AVRAMI MODEL TO CRYSTALLIZATION DATA

The classical Avrami equation

$$C(t) = 1 - e^{-Kt^n} \tag{1}$$

where $C(t)$ is the volume fraction crystallized at time t, K is the Avrami rate constant, and n is known as the Avrami exponent, was used to model the crys-

* Present address: Amoco Chemical Co., Naperville, IL.

† To whom correspondence should be addressed.

Journal of Applied Polymer Science, Vol. 45, 2005–2020 (1992)
 CCC 0021-8995/92/112005-16$04.00

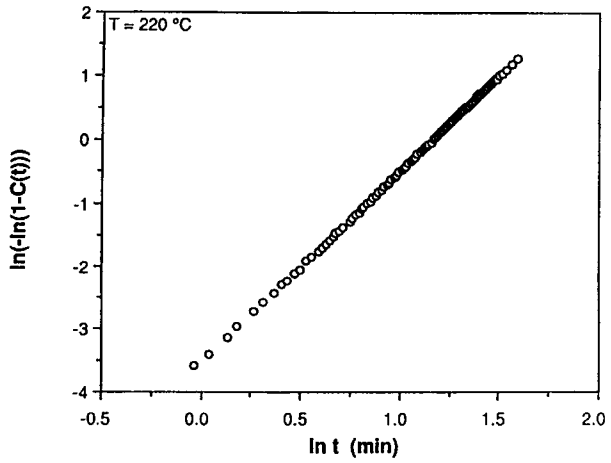

Figure 1 Avrami plot for isothermal crystallization of unreinforced PPS at 220°C.

tallization process for the composite systems described in Part I of this series.[1] Two types of crystallization behavior were typically observed. For unreinforced PPS, as well as for selected fiber-reinforced systems, the Avrami model adequately described the crystallization process in that the Avrami plot was linear for the entire range of volume fraction crystallized. A typical linear Avrami plot is shown in Figure 1. In other fiber-reinforced systems, however, deviations from a linear relationship were observed. A typical nonlinear Avrami plot is shown in Figure 2.

Listed in Table I are the systems studied along with the type of Avrami behavior observed. As can be seen, the aramid-reinforced systems exhibited nonlinear behavior, whereas the glass-reinforced systems exhibited linear Avrami behavior. The carbon-fiber systems exhibited both linear and nonlinear behavior depending on the type of carbon fiber used as the reinforcement. It is noteworthy that the Avrami behavior correlates with the observed morphology of the single-fiber thin-film specimens, as reported in Part I. Composites with reinforcing fibers that induced transcrystallinity (sized and unsized Kevlar 49, sized AS4, and graphitized Thornel) exhibited nonlinear Avrami behavior, while unreinforced PPS and composites with reinforcing fibers that did not induce transcrystallinity (unsized and sized glass and unsized AS4) exhibited linear Avrami behavior.

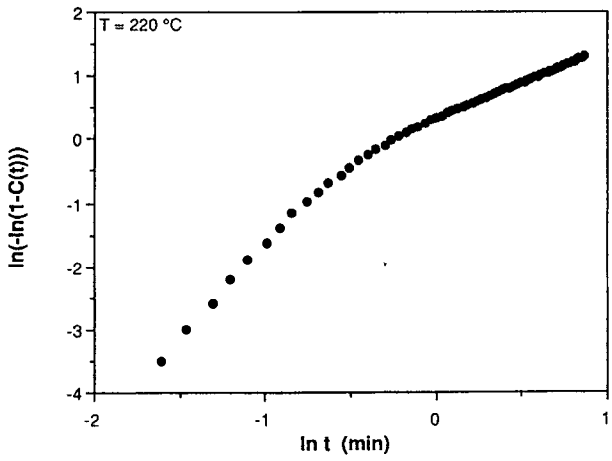

Figure 2 Avrami plot for isothermal crystallization of 53% sized Kevlar-reinforced PPS at 220°C.

Table I Type of Avrami Crystallization Behavior for PPS and Fiber-Reinforced PPS

System	Fiber Content (wt %)
Linear:	
Unreinforced PPS	–
Unsized AS4 carbon/PPS	18–54
Unsized glass/PPS	35–67
Sized glass/PPS	33–65
Commercial carbon prepreg	66
Commercial glass prepreg	70
Nonlinear:	
Sized AS4 carbon/PPS	39–64
Graphitized Thornel/PPS	20–65
Unsized Kevlar PPS	24–58
Sized Kevlar/PPS	22–53
Commercial aramid prepreg	55

LINEAR AVRAMI MODEL

Tabulated in Tables II and III are the values of the rate constant K and the Avrami exponent n for the systems studied at each of the isothermal crystallization temperatures. The systems listed at the top of the tables are those that exhibited linear Avrami plots, whereas the systems listed at the bottom of the tables are those that exhibited nonlinear Avrami behavior where we used the best-fit line to the data to compare the results to the linear systems. The values of the Avrami exponent for the linear systems range between 1.7 and 2.7, whereas for the nonlinear systems, the values of the exponent vary between 1.5 and 2.1, with the exception of the commercial aramid prepreg. The Avrami exponent was generally independent of the isothermal crystallization temperature, and it should also be noted that no significant systematic dependence of the Avrami exponent on fiber content was observed.

Table II Summary of Avrami Exponents for PPS and Fiber-Reinforced PPS Systems

System	220°C	225°C	230°C	235°C	240°C
Unreinforced PPS	2.7	2.6	2.4	2.4	2.2
Commercial glass (70%)	2.5	2.4	2.3	2.1	2.1
Unsized glass (35%)	2.5	2.5	2.4	2.3	2.3
Unsized glass (52%)	2.5	2.3	2.2	2.1	2.2
Unsized glass (67%)	1.9	2.0	1.9	1.8	1.9
Sized glass (33%)	2.5	2.4	2.2	2.3	2.3
Sized glass (48%)	2.5	2.4	2.3	2.4	2.3
Sized glass (65%)	1.8	1.7	1.8	2.0	1.8
Commercial carbon (66%)	2.5	2.5	2.4	2.3	2.3
Unsized AS4 (18%)	2.6	2.5	2.3	2.2	2.3
Unsized AS4 (28%)	2.2	2.1	2.0	2.1	1.8
Unsized AS4 (36%)	2.4	2.3	2.0	2.1	2.1
Unsized AS4 (46%)	1.7	1.8	2.0	2.0	2.1
Unsized AS4 (54%)	2.3	2.2	2.1	2.0	2.0
Sized AS4 (39%)	2.1	2.0	2.0	2.0	2.0
Sized AS4 (56%)	1.8	1.7	1.9	1.8	1.9
Sized AS4 (64%)	1.6	1.7	1.7	1.8	1.8
Graphitized Thornel (20%)	1.7	1.7	1.8	1.8	1.8
Graphitized Thornel (35%)	1.6	1.6	1.7	1.7	1.7
Graphitized Thornel (48%)	1.7	1.8	1.8	1.7	1.7
Graphitized Thornel (65%)	1.5	1.5	1.6	1.7	1.8
Commercial aramid (55%)	2.5	2.2	2.3	2.5	2.6
Unsized Kevlar 49 (24%)	1.6	1.7	1.6	1.8	1.9
Unsized Kevlar 49 (45%)	1.5	1.6	1.6	1.6	1.7
Unsized Kevlar 49 (58%)	1.7	1.7	1.6	1.7	1.7
Sized Kevlar 49 (22%)	1.7	1.6	1.6	1.7	1.8
Sized Kevlar 49 (34%)	1.3	1.5	1.6	1.8	2.2
Sized Kevlar 49 (43%)	1.4	1.5	1.5	1.7	1.8
Sized Kevlar 49 (53%)	1.6	1.7	1.7	2.0	2.1

Although there is a wide range of values for the Avrami rate constant (Table III), it is apparent that at any given crystallization temperature the systems exhibiting nonlinear Avrami behavior have higher values of the rate constant than do those systems that exhibited a linear Avrami relationship. For the nonlinear systems, the rate constants describe an average crystallization process because of the linear approximation.

Since the Avrami exponent is contained in the units for the rate constant, we recalculated the rate constants based on the observed crystallization half-time and an average value of the exponent. The crystallization half-time corresponds to a crystallized volume fraction of 0.5, and the Avrami equation can be manipulated into the following form:

$$K_0 = \frac{\ln 2}{t_{1/2}^n} \tag{2}$$

where $t_{1/2}$ is the crystallization half-time at a specified crystallization temperature and K_0 is the normalized Avrami rate constant. This normalization procedure was used only for those systems that exhibited linear Avrami behavior. With the calculation of normalized Avrami rate constants, we assumed an Arrhenius-type temperature dependence on the degree of undercooling from the thermodynamic crystallization temperature, i.e.,

$$K_0 = A_0 e^{-E_a/R\Delta T} \tag{3}$$

where E_a is an overall activation energy; A_0, an overall frequency factor; $\Delta T = (T_\infty - T)$, the degree of undercooling from the thermodynamic equilibrium crystallization temperature T_∞; and R, the universal gas constant. T_∞ for PPS, 303°C, was taken from the work of Lovinger et al.[11] A typical Arrhenius plot is shown in Figure 3 for the 67%

Table III Average Values for the Avrami Rate Constant at Each of the Crystallization Temperatures Investigated

System	220°C	225°C	230°C	235°C	240°C
Unreinforced PPS	43.6	17.6	7.6	2.5	0.9
Commercial glass (70%)	31.3	13.4	7.1	3.1	1.7
Unsized glass (35%)	45.8	19.9	10.1	3.9	1.0
Unsized glass (52%)	52.0	25.0	11.9	4.8	1.2
Unsized glass (67%)	48.3	26.5	13.3	6.1	2.2
Sized glass (33%)	47.4	22.4	11.2	3.6	1.5
Sized glass (48%)	65.5	28.6	14.1	4.1	1.4
Sized glass (65%)	58.9	37.6	19.2	9.7	4.0
Commercial carbon (66%)	107.0	39.3	14.5	6.9	2.0
Unsized AS4 (18%)	73.1	32.4	12.0	6.6	1.7
Unsized AS4 (28%)	28.6	8.6	4.9	1.4	1.0
Unsized AS4 (36%)	4.7	1.9	2.4	0.5	0.2
Unsized AS4 (46%)	52.7	29.4	13.6	5.1	2.1
Unsized AS4 (54%)	105.0	50.1	13.6	5.1	2.1
Sized AS4 (39%)	111.0	59.5	27.1	10.2	5.7
Sized AS4 (56%)	119.0	66.5	34.3	14.7	4.9
Sized AS4 (64%)	150.0	81.5	47.5	17.6	9.9
Graphitized Thornel (20%)	479.0	337.0	154.0	79.6	45.2
Graphitized Thornel (35%)	1100.0	555.0	304.0	147.0	64.1
Graphitized Thornel (48%)	720.0	405.0	208.0	101.0	50.4
Graphitized Thornel (65%)	723.0	518.0	336.0	167.0	88.8
Commercial aramid (55%)	1570.0	554.0	279.0	64.7	8.3
Unsized Kevlar 49 (24%)	292.0	145.0	75.3	28.7	12.3
Unsized Kevlar 49 (45%)	460.0	250.0	140.0	71.0	21.0
Unsized Kevlar 49 (58%)	297.0	146.0	83.4	39.4	15.3
Sized Kevlar 49 (22%)	271.0	147.0	79.0	30.1	10.7
Sized Kevlar 49 (34%)	785.0	502.0	257.0	74.1	16.4
Sized Kevlar 49 (43%)	595.0	375.0	190.0	79.1	25.1
Sized Kevlar 49 (53%)	1100.0	612.0	338.0	119.0	27.0

All values have been multiplied by 10^3. Units of K are $(\text{min})^{-n}$.

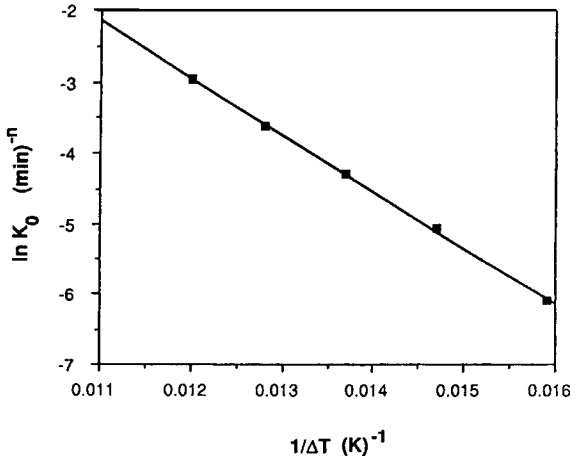

Figure 3 Arrhenius dependence of rate constant for 67% unsized glass-reinforced PPS.

unsized glass-reinforced PPS system. The overall activation energy, as determined from the slope of the best-fit line to the data, and the overall frequency factor, as determined from the intercept of the best-fit line, for the systems that exhibited linear Avrami behavior are given in Table IV.

Further insight can be obtained by analyzing the relative contributions of nucleation and crystal growth to the crystallization process. Consider that the Avrami rate constant is composed of contributions from nucleation and crystal-growth processes. Since the Avrami rate constant must have units of reciprocal time raised to the value of the Avrami exponent, and both the nucleation rate (N^*) and the growth rate (G) have units of reciprocal time, the Avrami rate constant can be expressed in the following manner:

Table IV Arrhenius Dependence of Normalized Rate Constants for Model Composites with the Most Nearly Equal High-Fiber Contents of Systems Exhibiting Linear Avrami-Type Crystallization Behavior

System	n	E_a (kcal/mol)	E_g (kcal/mol)	A_0 $(\text{min})^{-n}$	A_g (min)
PPS (molded)	2.5	2.1	0.9	13.50×10^3	50
Unsized glass (67%)	1.9	1.6	0.9	0.92×10^3	40
Sized glass (65%)	1.8	1.5	0.8	0.46×10^3	30
Unsized AS4 (54%)	2.1	1.6	0.8	1.35×10^3	30

The average value of the Avrami exponent for the temperature range studied was used in the calculation of the normalized rate constant according to eq. (2).

$$K_0 = N^{*x} G^{(n-x)} \tag{4}$$

where x is the relative contribution of the nucleation rate to the rate constant and $(n - x)$ is the relative contribution of the growth rate to the rate constant. Furthermore, the nucleation and the crystal-growth rates are presumed to follow an Arrhenius temperature dependence:

$$N^* = \mathrm{A}_* e^{-E_*/R\Delta T} \tag{5}$$

$$G = A_g e^{-E_g/R\Delta T} \tag{6}$$

where A_* and A_g are the frequency factors for nucleation and growth and E_* and E_g are the corresponding activation energies. If eqs. (5) and (6) are substituted into eq. (4), the following result is obtained:

$$K_0 = A_*^x e^{-xE_*/\mathrm{R}\Delta\mathrm{T}} A_g^{(n-x)} e^{-(n-x)E_g/R\Delta T} \tag{7}$$

which leads to

$$\ln K_0 = \ln A_*^x A_g^{(n-x)} - \frac{x(E_n - E_g) + nE_g}{R} \frac{1}{\Delta T} \tag{8}$$

Equation (8) indicates that the overall activation energy and overall frequency factor can be expressed in terms of contributions from the nucleation and growth-activation energies and frequency factors. The resulting relationships are

$$E_a = x(E_* - E_g) + nE_g \tag{9}$$

$$A_0 = A_*^x A_g^{(n-x)} \tag{10}$$

Referring to Table II, the average of all the Avrami exponents for the linear systems is close to a value of 2, which may be interpreted as two-dimensional crystal growth with a linear growth rate and the crystals nucleating athermally. If this interpretation is correct, then the athermal nucleation implies that there is no contribution from the nucleation rate to the activation energy. In other words, the value of x in eqs. (9) and (10) is equal to zero and the only contribution to E_a is from the crystal-growth process. Equations (9) and (10) can then be rearranged to provide the activation energy and the frequency factor for crystal growth in the following manner:

$$E_g = \frac{E_a}{n} \tag{11}$$

$$A_g = A_0^{1/n} \tag{12}$$

The relevant quantities are given in Table IV, and it is apparent that the activation energies for crystal growth are similar for the different systems. This is reasonable since the matrix polymer, PPS, is the same in each of the systems. Also, the activation energies observed for crystal growth correlate reasonably well with the prediction of Lovinger et al.,[11] for the activation energy of low molecular weight PPS molecular chain motion. They report an activation energy for 15,000 M_w PPS of 1.4 kcal/mol.

The different values obtained for the overall frequency factors, A_0, listed in Table IV are a reflection of the differing contributions of nucleation and crystal growth to the frequency factor. Although there is no effect of nucleation rate, due to the assumption of athermal nucleation, the presence and type of fiber reinforcement affects the number and distribution of athermal nuclei. Presumably, the overall frequency factor reflects the nucleation density of athermal nuclei, as well as the variations in the crystal-growth rate and growth habit that arise due to the constraints imposed on the growing polymer crystals by the fibers.

NONLINEAR AVRAMI BEHAVIOR—PARALLEL MODEL

For the fiber-reinforced PPS systems that exhibited nonlinear Avrami behavior and that produce a transcrystalline morphology in the thin-film studies, the crystallization data were approximated by two linear regions, as shown for PPS reinforced with 53% sized Kevlar at 220°C in Figure 4. We assume that the two processes are the crystallization of the bulk-nucleated spherulites and the formation of crystals nucleated at the fiber surface. We use the parallel Avrami model originally proposed by Velisaris and Seferis,[6] which contains an Avrami contribution for each of the two crystallization processes and which may be expressed as

$$C(t) = w(1 - e^{-K_1 t^{n_1}}) + (1 - w)(1 - e^{-K_2 t^{n_2}}) \quad (13)$$

where w is the volume fraction of material crystallized by the first process, n_1 and K_1 are the Avrami parameters for the first process, and n_2 and K_2 are the Avrami parameters for the second process.

The five parameters in eq. (13) were evaluated using a nonlinear numerical regression scheme. A typical best-fit curve of eq. 13 to the experimentally determined volume fraction crystallized is shown in Figure 5. The average values for each of the five parameters yielding the best fit are listed in Table V for a crystallization temperature of 220°C, and in Table VI, for a crystallization temperature of 240°C for the most nearly equal high-fiber loadings of the four systems that exhibited nonlinear Avrami behavior. Although data for only two temperatures are presented, the analysis was performed for all of the crystallization temperatures.

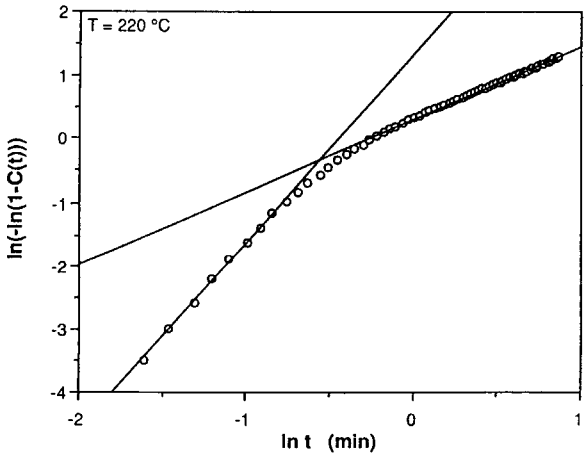

Figure 4 Avrami plot for 53% sized Kevlar-reinforced PPS crystallized at 220°C.

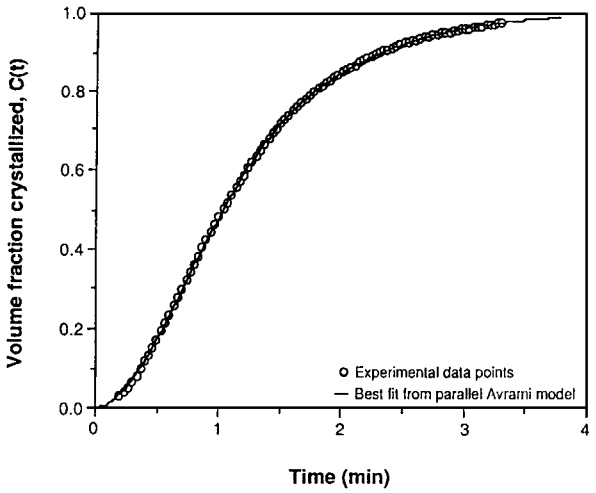

Figure 5 Best-fit curve obtained from five parameter parallel Avrami model for 65% Thornel-reinforced PPS isothermally crystallized at 220°C.

The average value of the Avrami exponent for the first process over the temperature range studied was 2.5, whereas the average value for the second process was 2.0. The exponent 2.0 for the second process can be interpreted, as in the preceding section, as reflecting two-dimensional spherulitic growth of athermally nucleated crystals. The exponent 2.5 is more difficult to interpret. Wunderlich[12] associates a value of 2.5 with three-dimensional spherulitic growth of thermally nucleated crystals, with the growth rate being controlled by heat removal from the growing crystal front. In light of the morphological observations, it appears unreasonable to apply this interpretation to the formation of the transcrystalline region, since nucleation of the transcrystalline region appears to be athermal. A more reasonable explanation for the 2.5 value of the exponent is that there is a distribution of two- and three-dimensional crystal growth due to the distribution of interfiber spacing in the composite.

Since two different crystallization processes have been proposed, the related crystallization half-times can be calculated by rearranging eq. (2) into the following form:

$$t_{1/2} = \left(\frac{\ln 2}{K_{1,2}}\right)^{1/n_{1,2}} \quad (14)$$

The calculated crystallization half-times for the first

Table V Average Values of Best-Fit Parameters to Parallel Avrami Model for Isothermal Crystallization at 220°C

System	w	n_1	K_1 $(\text{min})^{-n}$	n_2	K_2 $(\text{min})^{-n}$
Sized AS4 (64%)	0.427	2.5	0.22	1.9	0.72×10^{-1}
Thornel (65%)	0.369	2.1	2.37	1.8	4.59×10^{-1}
Unsized Kevlar (58%)	0.390	2.1	0.91	1.9	2.39×10^{-1}
Sized Kevlar (53%)	0.545	2.7	4.15	1.8	6.55×10^{-1}

Table VI Average Values of Best-Fit Parameters to Parallel Avrami Model for Isothermal Crystallization at 240°C

System	w	n_1	K_1 $(\text{min})^{-n}$	n_2	K_2 $(\text{min})^{-n}$
Sized AS4 (64%)	0.318	2.2	0.55×10^{-2}	1.9	0.49×10^{-2}
Thornel (65%)	0.562	2.4	10.40×10^{-2}	2.0	4.46×10^{-2}
Unsized Kevlar (58%)	0.446	2.6	1.00×10^{-2}	2.0	0.85×10^{-2}
Sized Kevlar (53%)	0.585	2.8	2.50×10^{-2}	2.4	1.06×10^{-2}

process are always lower than those for the second process, indicating that the first process occurs at a faster rate. The crystallization half-times for the two crystallization processes for the 65% graphitized Thornel carbon system are shown in Figure 6. The three other nonlinear systems exhibited similar behavior. The lower crystallization half-time for the first process supports the assumption that the first process is the formation of the transcrystalline region, whereas the second process is the formation of spherulitic crystals.

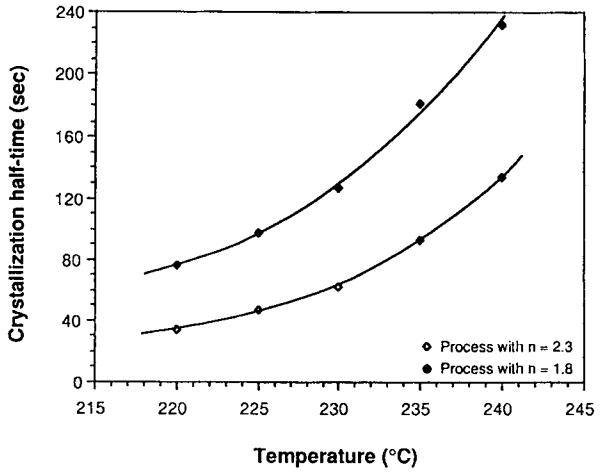

Figure 6 Crystallization half-time for each of the processes in the parallel Avrami model as a function of isothermal crystallization temperature for 65% Thornel-reinforced PPS.

The temperature dependence of the rate constants for the two processes was investigated by assuming an Arrhenius dependence on the degree of undercooling as in the analysis presented in the preceding section. The Arrhenius dependencies for the case of the 58% unsized Kevlar-reinforced PPS system are shown in Figure 7. As can be seen, both processes follow a linear relationship, indicating that the Arrhenius dependence for each process is reasonable.

The activation energies and frequency factors found for each of the processes in the parallel model are given in Table VII, along with the previously reported values for those systems that exhibited linear Avrami behavior. The results indicate that the overall activation energies, as well as the activation energies for crystal growth, for each of the two processes are nearly the same and are similar to the activation energies for the linear Avrami systems. Differences in the frequency factors are presumed to be related to differences in the number of athermal nuclei. The higher values of the frequency factors for the first process as compared to the second process indicate that, since the crystal growth rates for the two processes are similar, the nucleation density of the fiber surface is higher than the nucleation density in the bulk polymer.

Although it is apparent that the parallel Avrami model can be used to model the development of the

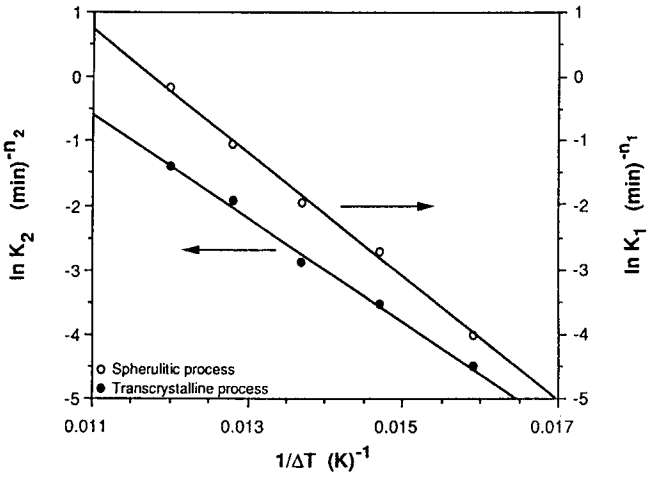

Figure 7 Arrhenius dependence of the rate constants on the degree of undercooling for each of the two processes in the parallel Avrami model for 58% unsized Kevlar-reinforced PPS.

volume fraction crystallized (see Fig. 5), the interpretation of the results has certain deficiencies. The assumption that the first process corresponds to the development of a transcrystalline morphology while the second process corresponds to the spherulitic morphology was based on the values of the Avrami exponent and the observation that the crystallization half-times for the first process were lower than those for the second process. A factor that was not considered in the interpretation but must not be overlooked is the effect of interfiber spacing. At the high-fiber contents of these systems, the interfiber spacing is relatively small. On average, the interfiber spacing is approximately 6 μm. If the assumption of a dual morphology in these small interfiber spaces is valid, then the parallel model can be used to calculate the relative contents of transcrystalline and spherulitic morphologies. Based on the calculated relative volume fractions, the transcrystalline region would extend 1.3 μm from the fiber surface and the average spherulite diameter would be 2.6 μm. However, based on the morphological observations of the transcrystalline regions,[1] transcrystallinity is observed to extend at least 10 μm from the fiber surface. In fact, Figure 8 demonstrates that at small interfiber spacings only transcrystalline morphology is present. If this is the case, then the underlying interpretation of the parallel model cannot be valid.

NONLINEAR AVRAMI BEHAVIOR—SERIES MODEL

As an alternative to the parallel Avrami model, our kinetic data can be treated in terms of a series model involving two sequential processes, as shown in Figure 9. Here we assume that the first process is related to the formation of the transcrystalline region,

Table VII Arrhenius Temperature Dependence of Rate Constants Obtained from Parallel Avrami Model and Activation Energies and Frequency Factors for the Linear Avrami Systems

System	n_1	E_{a_1} (kcal/mol)	E_{g_1} (kcal/mol)	A_{K_1} $(\text{min})^{-n}$	A_{g_1} (min)	n_2	E_{a_2} (kcal/mol)	E_{g_2} (kcal/mol)	A_{K_2} $(\text{min})^{-n}$	A_{g_2} (min)
Molded PPS						2.5	2.1	0.9	13.50×10^3	50
Unsized AS4 (54%)						2.1	1.6	0.8	1.35×10^3	30
Sized AS4 (64%)	2.4	2.1	0.9	6.66×10^4	110	1.9	1.3	0.7	0.16×10^3	10
Thornel (65%)	2.3	1.6	0.7	3.96×10^4	110	1.8	1.1	0.6	0.33×10^3	20
Unsized glass (67%)						1.9	1.6	0.9	0.92×10^3	40
Sized glass (65%)						1.8	1.5	0.8	0.46×10^3	30
Unsized Kevlar (58%)	2.3	1.9	0.8	9.67×10^4	150	1.9	1.6	0.9	4.97×10^3	90
Sized Kevlar (53%)	2.7	2.6	1.0	40.50×10^6	610	2.0	1.8	0.9	35.50×10^3	170

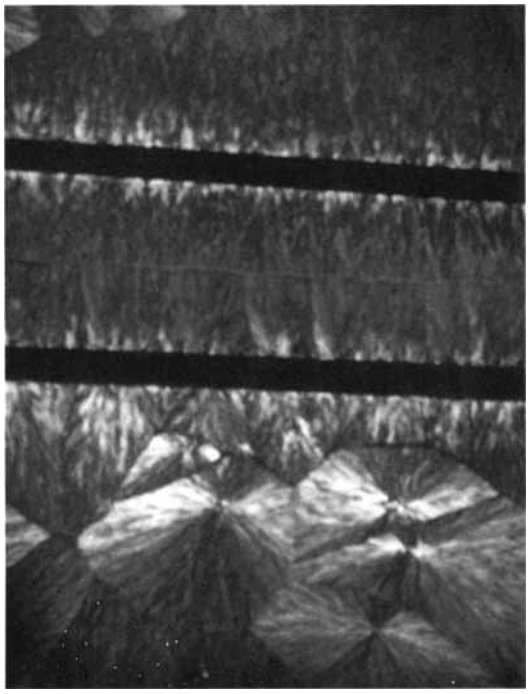

Figure 8 Polarizing light photomicrograph of a model thin-film composite of sized AS4 carbon fibers in a PPS matrix (magnification 570×).

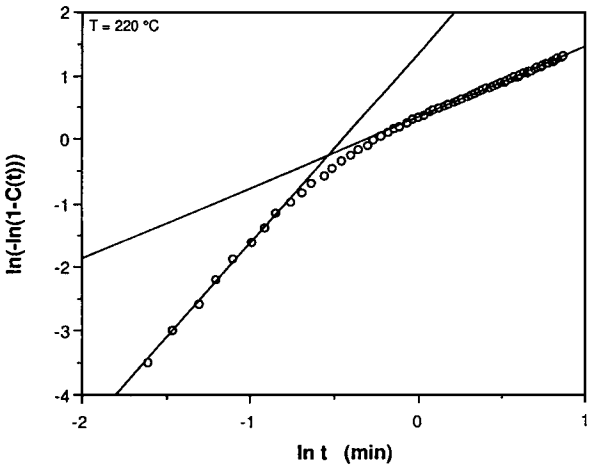

Figure 9 Avrami plot for 53% sized Kevlar-reinforced PPS crystallized at 220°C using two linear processes in series to model the observed behavior.

whereas the second process is secondary crystallization. We treat both processes according to the standard Avrami equation to obtain rate constants and Avrami exponents that are summarized in Tables VIII and IX for crystallizations at 220 and 240°C, respectively. The intersection of the two linear regions was considered to be the point at which the crossover from the first process to the second process occurs. This crossover occurs at a higher volume fraction crystallized at the higher crystallization temperature, indicating that less secondary crystallization takes place. Presumably, the rate of the primary crystallization process is slow enough at the higher temperature so that a higher amount of primary crystallization can occur.

One of the more interesting results from this model comes from the calculation of the crystallization half-times from the Avrami rate constants and exponents for each of the processes. For all the composite systems, the crystallization half-time for the first process was approximately the same as that for the second process. A typical plot of the crystallization half-times as function of crystallization temperature is shown in Figure 10 for the 65% graphitized Thornel-reinforced PPS. The implication of this finding is that the overall crystallization rates for the two processes are similar, but the second process has a longer induction time than the first. Intuitively, this would seem reasonable since the secondary crystallization process cannot occur until the primary crystal structure has been formed.

The temperature dependence of the rate constants for both processes was postulated to follow

Table VIII Average Values of Best-Fit Parameters to Series Avrami Model for Isothermal Crystallization at 220°C

System	C	n_1	K_1 $(\text{min})^{-n}$	n_2	K_2 $(\text{min})^{-n}$
Sized AS4 (64%)	0.401	2.4	1.58×10^{-1}	1.3	2.93×10^{-1}
Thornel (65%)	0.399	2.1	13.30×10^{-1}	1.2	8.25×10^{-1}
Unsized Kevlar (58%)	0.285	2.3	4.22×10^{-1}	1.5	3.79×10^{-1}
Sized Kevlar (53%)	0.537	3.0	40.10×10^{-1}	1.1	14.00×10^{-1}

The value of the volume fraction crystallized that corresponds to the crossover from the primary process to the secondary process is indicated in the column denoted as C.

Table IX Average Values of Best-Fit Parameters to Series Avrami Model for Isothermal Crystallization at 240°C

System	C	n_1	K_1 $(\text{min})^{-n}$	n_2	K_2 $(\text{min})^{-n}$
Sized AS4 (64%)	0.452	2.1	0.07×10^{-1}	1.4	0.40×10^{-1}
Thornel (65%)	0.416	2.5	0.67×10^{-1}	1.4	2.04×10^{-1}
Unsized Kevlar (58%)	0.305	2.2	0.10×10^{-1}	1.5	0.32×10^{-1}
Sized Kevlar (53%)	0.656	2.7	0.27×10^{-1}	1.5	1.36×10^{-1}

The value of the volume fraction crystallized which corresponds to the crossover from the primary process to the secondary process is indicated in the column denoted as C.

an Arrhenius relationship, and activation energies for the first and second processes were calculated. A typical Arrhenius dependence of the rate constants on the degree of undercooling is shown in Figure 11 for the 64% sized AS4-reinforced PPS system; similar results were obtained for all the nonlinear Avrami composites (Table I). The values for the activation energies and frequency factors are displayed in Table X along with the previously reported results for the linear Avrami systems. The overall activation energies for the first process are somewhat higher than those for the second process. When the overall activation energies are normalized by the corresponding Avrami exponents, the activation energies are similar, indicating that this activation energy (E_{g1}) is related to the growth of the crystal structure.

It is of interest that the Arrhenius dependence of the rate constants from the series model yielded results similar to those obtained from the linear Avrami systems as well as from the parallel Avrami model, indicating that on a fundamental level the activation energy for crystal growth is a measure of the activation energy for molecular chain motion to the growing crystal surface. While the Arrhenius analysis of the parallel and series Avrami models provided similar results, one must keep in mind that the fundamental interpretation of the two models is quite different. In the parallel model, the two processes are assumed to correspond to the formation of two different crystal morphologies, while in the series model, only one type of morphology is visualized.

CRYSTALLINITY MODEL

While the classical Avrami analysis is useful in describing the volume fraction crystallized and in in-

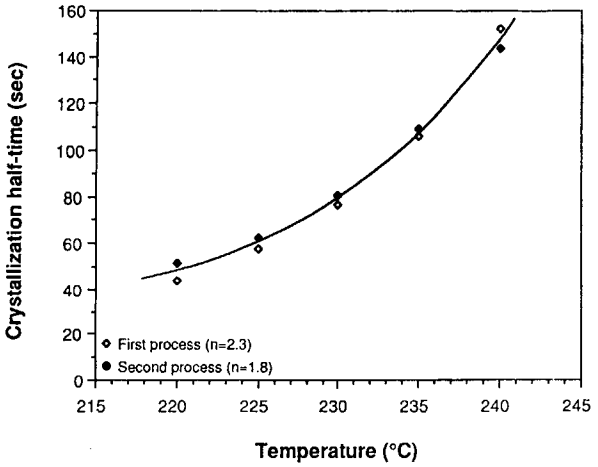

Figure 10 Crystallization half-time as a function of isothermal crystallization temperature for 65% Thornel-reinforced PPS as determined from the Avrami rate constants and exponents of two Avrami processes occurring in series.

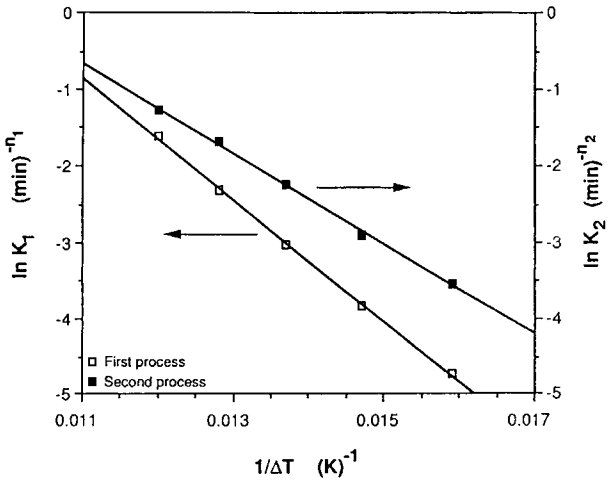

Figure 11 Arrhenius dependence of rate constants for 64% sized AS4 carbon fiber-reinforced PPS determined from series Avrami model.

Table X Arrhenius Temperature Dependence of Rate Constants Obtained from Series Avrami Model and Activation Energies and Frequency Factors for the Linear Avrami Systems

System	n_1	E_{a_1} (kcal/mol)	E_{g_1} (kcal/mol)	A_{K_1} $(\text{min})^{-n}$	A_{g_1} (min)	n_2	E_{a_2} (kcal/mol)	E_{g_2} (kcal/mol)	A_{K_2} $(\text{min})^{-n}$	A_{g_2} (min)
Molded PPS	2.5	2.1	0.9	13.50×10^3	50					
Unsized AS4 (54%)	2.1	1.6	0.8	1.35×10^3	30					
Sized AS4 (64%)	2.3	1.6	0.7	2.90×10^3	30	1.4	1.2	0.8	3.45×10^2	70
Thornel (65%)	2.3	1.5	0.6	11.60×10^3	60	1.3	0.9	0.6	1.61×10^2	50
Unsized Glass (67%)	1.9	1.6	0.9	0.92×10^3	40					
Sized Glass (65%)	1.8	1.5	0.8	0.46×10^3	30					
Unsized Kevlar (58%)	2.3	1.9	0.9	55.80×10^3	130	1.5	1.3	0.9	8.70×10^2	100
Sized Kevlar (53%)	3.0	2.6	0.9	298.00×10^5	330	1.2	1.2	1.0	25.40×10^2	830

terpreting the overall rate of crystallization, the Avrami analysis does not account for the development of absolute crystallinity, i.e., while the material may be fully crystallized in kinetic terms, it is not fully crystalline in thermodynamic terms. It would seem appropriate to correct the volume fraction crystallized by the ultimate degree of crystallinity to account for structural imperfections and residual amorphous content. In this way, we obtain

$$X(t) = C(t)X(t_c) \quad (15)$$

where $X(t)$ is the absolute crystallinity at time t; $C(t)$, the volume fraction crystallized at time t; and $X(t_c)$, the degree of crystallinity at the completion of the crystallization process.

We analyzed our kinetic data by an equation analogous to the classical Avrami model, as follows:

$$X(t) = 1 - e^{-K_c t^{n_c}} \quad (16)$$

where K_c is the rate constant for the development of absolute crystallinity and n_c is the exponent of time in the equation. Equation (16) can be rearranged into the following form:

$$\ln\{-\ln[1 - X(t)]\} = \ln K_c + n_c \ln t \quad (17)$$

which is analogous to the linear Avrami model. Figures 12, 13, and 14 for unreinforced PPS, 67% unsized glass fiber-reinforced PPS, and 53% sized Kevlar 49 reinforced PPS, respectively, display the typical behavior observed. All the systems, at each of the temperatures investigated, exhibited the type of behavior displayed in these figures in that the relationships were initially linear followed by a roll-off that at longer times could be approximated by a linear relationship. We used a series model involving two linear relationships to obtain the intersection point of the two processes as well as the corresponding rate constants and exponents. The results are

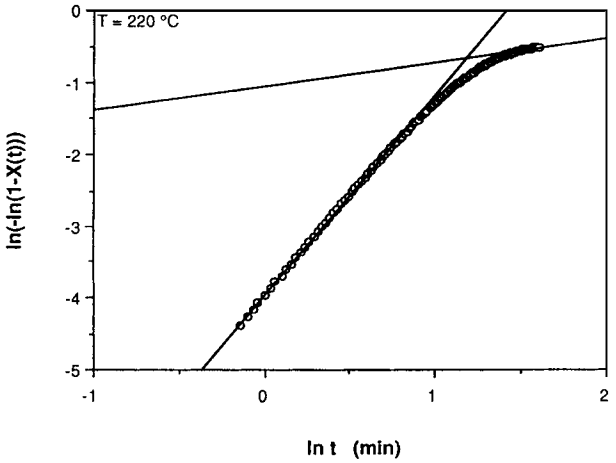

Figure 12 Determination of Avrami rate constants and exponents based on the series crystallinity model for unreinforced PPS crystallized at 220°C.

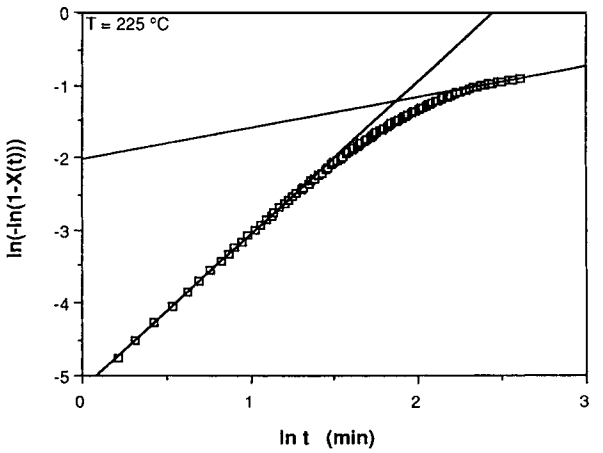

Figure 13 Determination of Avrami rate constants and exponents based on the series crystallinity model for 67% unsized glass fiber-reinforced PPS crystallized at 225°C.

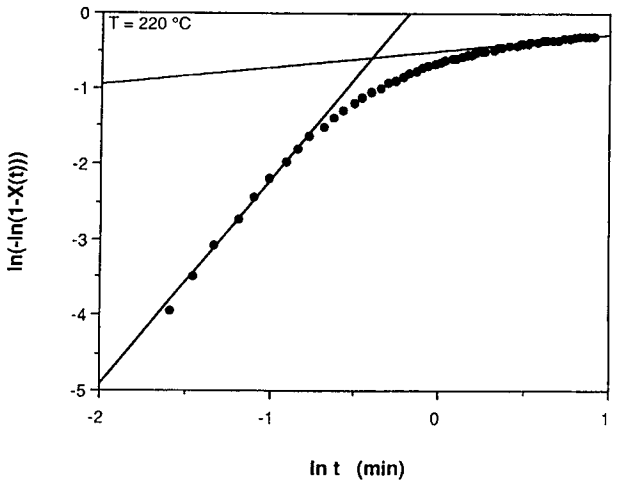

Figure 14 Determination of Avrami rate constants and exponents based on the series crystallinity model for 53% sized Kevlar-reinforced PPS crystallized at 220°C.

summarized in Tables XI–XV. Also listed in these tables are the fractions (in %) of the absolute crystallinity levels that develop during the primary crystallization process. This was calculated from the crystallinity value at which the crossover from the primary process to the secondary process occurred, then normalizing that by the ultimate crystallinity.

As can be seen from the data presented in Tables XI–XV, the values for the exponent of the second crystallization process are extremely consistent and average 0.4, whereas the values for the first process vary from 1.9 to 3.3. The large variation in the exponent for the first process is presumed to be due to the effect of the different fiber surfaces on the primary crystallization process, while the consistency in the second exponent reflects the crystallite perfection and/or secondary crystallization processes that would be expected to be independent of the type of fiber present. It is of interest that those systems that exhibited a spherulitic morphology with no transcrystallinity (molded PPS, unsized and sized glass, and unsized AS4), a higher fraction of the crystallinity generally developed during the primary crystallization process than for those systems that exhibited a transcrystalline morphology (unsized and sized Kevlar, sized AS4, and Thornel). This indicates that more secondary crystallization and crystallite perfection is occurring in the systems

Table XI Average Values of Best-Fit Parameters to Crystallinity Model for Isothermal Crystallization at 220°C

System	n_{c1}	K_{c1} $(\text{min})^{-n}$	n_{c2}	K_{c2} $(\text{min})^{-n}$	% Primary
PPS (molded)	2.8	0.17×10^{-1}	0.5	2.45×10^{-1}	84.0
Unsized glass (67%)	2.2	0.15×10^{-1}	0.4	2.04×10^{-1}	75.5
Sized glass (65%)	2.4	0.15×10^{-1}	0.4	2.17×10^{-1}	70.5
Unsized AS4 (54%)	2.4	0.53×10^{-1}	0.3	4.44×10^{-1}	85.5
Sized AS4 (64%)	2.4	0.64×10^{-1}	0.4	2.79×10^{-1}	67.0
Thornel (65%)	2.0	7.09×10^{-1}	0.4	3.30×10^{-1}	60.1
Unsized Kevlar (58%)	2.3	2.72×10^{-1}	0.4	3.02×10^{-1}	66.6
Sized Kevlar (53%)	2.9	18.70×10^{-1}	0.2	6.08×10^{-1}	77.4

Table XII Average Values of Best-Fit Parameters to Crystallinity Model for Isothermal Crystallization at 225°C

System	n_{c1}	K_{c1} $(\text{min})^{-n}$	n_{c2}	K_{c2} $(\text{min})^{-n}$	% Primary
PPS (molded)	2.6	0.79×10^{-2}	0.5	2.12×10^{-1}	82.3
Unsized glass (67%)	2.1	0.84×10^{-2}	0.4	1.67×10^{-1}	85.0
Sized glass (65%)	2.3	0.79×10^{-2}	0.4	1.87×10^{-1}	70.8
Unsized AS4 (54%)	2.3	2.60×10^{-2}	0.3	3.62×10^{-1}	81.7
Sized AS4 (64%)	2.2	3.20×10^{-2}	0.5	2.25×10^{-1}	67.0
Thornel (65%)	2.2	25.20×10^{-2}	0.3	2.93×10^{-1}	70.6
Unsized Kevlar (58%)	2.3	9.52×10^{-2}	0.4	2.42×10^{-1}	64.4
Sized Kevlar (53%)	3.3	62.30×10^{-2}	0.2	5.43×10^{-1}	76.7

Table XIII Average Values of Best-Fit Parameters to Crystallinity Model for Isothermal Crystallization at 230°C

System	n_{c1}	K_{c1} $(\text{min})^{-n}$	n_{c2}	K_{c2} $(\text{min})^{-n}$	% Primary
PPS (molded)	2.5	0.39×10^{-2}	0.5	1.72×10^{-1}	81.9
Unsized glass (67%)	2.1	0.39×10^{-2}	0.4	1.44×10^{-1}	75.4
Sized glass (65%)	2.3	0.40×10^{-2}	0.4	1.52×10^{-1}	71.1
Unsized AS4 (54%)	2.2	1.31×10^{-2}	0.3	3.39×10^{-1}	83.9
Sized AS4 (64%)	2.3	1.48×10^{-2}	0.5	1.87×10^{-1}	68.1
Thornel (65%)	2.3	14.60×10^{-2}	0.3	2.46×10^{-1}	68.9
Unsized Kevlar (58%)	2.3	3.49×10^{-2}	0.3	2.19×10^{-1}	66.3
Sized Kevlar (53%)	3.1	16.90×10^{-2}	0.2	4.50×10^{-1}	76.2

Table XIV Average Values of Best-Fit Parameters to Crystallinity Model for Isothermal Crystallization at 235°C

System	n_{c1}	K_{c1} $(\text{min})^{-n}$	n_{c2}	K_{c2} $(\text{min})^{-n}$	% Primary
PPS (molded)	2.3	1.75×10^{-3}	0.5	1.50×10^{-1}	84.9
Unsized glass (67%)	2.1	1.85×10^{-3}	0.4	1.17×10^{-1}	77.8
Sized glass (65%)	2.3	1.71×10^{-3}	0.4	1.25×10^{-1}	72.6
Unsized AS4 (54%)	2.0	6.53×10^{-3}	0.2	2.74×10^{-1}	85.1
Sized AS4 (64%)	2.2	5.24×10^{-3}	0.5	1.58×10^{-1}	68.5
Thornel (65%)	2.5	53.40×10^{-3}	0.3	2.00×10^{-1}	71.8
Unsized Kevlar (58%)	2.2	12.60×10^{-3}	0.4	1.56×10^{-1}	64.4
Sized Kevlar (53%)	2.9	47.40×10^{-2}	0.3	3.73×10^{-1}	78.6

with transcrystallinity than in the spherulitic systems. In all systems, however, the amount of crystallinity developed during the primary process is quite high, with an average for all systems of 72% of the absolute crystallinity developing during the primary crystallization process.

We again investigated the Arrhenius temperature dependence of the rate constants for each of the two crystallization processes, and typical results are shown in Figure 15 for unreinforced PPS and in Figure 16 for 64% sized AS4-reinforced PPS. Overall activation energies and frequency factors were determined for both processes and are reported in Table XVI, along with the activation energies and frequency factors based on the assumption of athermal nucleation; i.e., activation energies and frequency

Table XV Average Values of Best-Fit Parameters to Crystallinity Model for Isothermal Crystallization at 240°C

System	n_{c1}	K_{c1} $(\text{min})^{-n}$	n_{c2}	K_{c2} $(\text{min})^{-n}$	% Primary
PPS (molded)	2.3	0.42×10^{-3}	0.5	1.15×10^{-1}	75.7
Unsized glass (67%)	1.9	1.06×10^{-3}	0.5	0.99×10^{-1}	77.4
Sized glass (65%)	2.0	0.82×10^{-3}	0.5	0.94×10^{-1}	70.6
Unsized AS4 (54%)	2.0	2.69×10^{-3}	0.3	2.19×10^{-1}	80.8
Sized AS4 (64%)	2.0	2.14×10^{-3}	0.4	1.25×10^{-1}	67.6
Thornel (65%)	2.5	22.00×10^{-3}	0.4	1.54×10^{-1}	64.9
Unsized Kevlar (58%)	2.2	5.05×10^{-3}	0.4	1.29×10^{-1}	66.5
Sized Kevlar (53%)	2.8	12.30×10^{-2}	0.4	2.85×10^{-1}	66.7

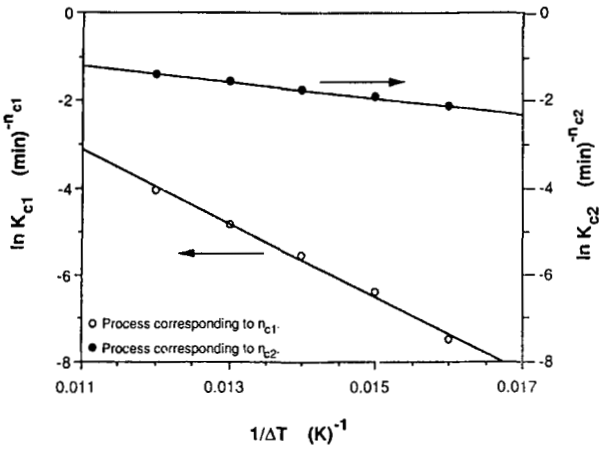

Figure 15 Arrhenius dependence of rate constants for unreinforced PPS based on the series crystallinity model.

factors were determined in a manner analogous to eqs. (11) and (12) using the exponent of time n_{c1}. However, in this crystallinity model, there is no fundamental basis for assigning nucleation and growth contributions to the rate constant. In fact, the development of absolute crystallinity should arise only from the growing crystals since the nuclei presumably contribute only minor amounts of crystallinity to the overall crystallinity.

One of the most encouraging aspects of this model is the description that it provides of secondary crystallization. The overall activation energy, E_{ec2}, and the overall frequency factor, A_{Kc2}, are nearly the same for all the systems, confirming that secondary crystallization and crystallite perfection are independent of the type of reinforcing fiber. From a mechanistic viewpoint, this is reasonable since crystal perfection should be dependent only on the ability of the polymer chains to move or fold into favorable configurations. This segmental motion would be expected to depend on the crystallization temperature but not on the type of fiber reinforcement. Certainly, the fiber surface would appear to have a larger effect on the primary crystallization process, since the nucleation density of the fiber surface determines the type of crystal structure formed.

The frequency factors for the first process are indicative of the nucleating abilities of the fiber surfaces and the influences on the crystal-growth rate. The systems that exhibited surface-nucleated crystals (transcrystallinity) have higher values of the frequency factor than those systems that did not exhibit transcrystallinity. Within the transcrystalline systems, the frequency factors provide insight into the mechanisms of crystallization. The sized Kevlar system is observed to have a higher frequency factor than the unsized Kevlar system, indicating that the size enhances the growth rate of the crystal structure. This is consistent with data we reported in a previous paper on the effects of fibers on the glass-transition temperature of PPS.[13]

Based on this crystallinity model, we can postulate a mechanistic description of the crystallization process for those systems that exhibit transcrystallinity. Since transcrystallinity is presumed to be a surface-nucleated phenomenon, the nucleation

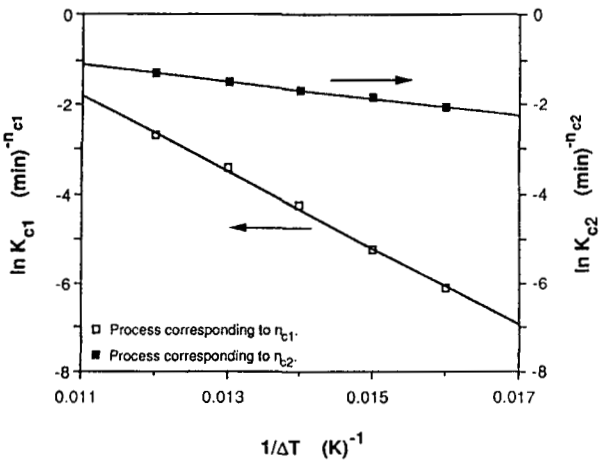

Figure 16 Arrhenius dependence of rate constants for 64% sized AS4-reinforced PPS based on the series crystallinity model.

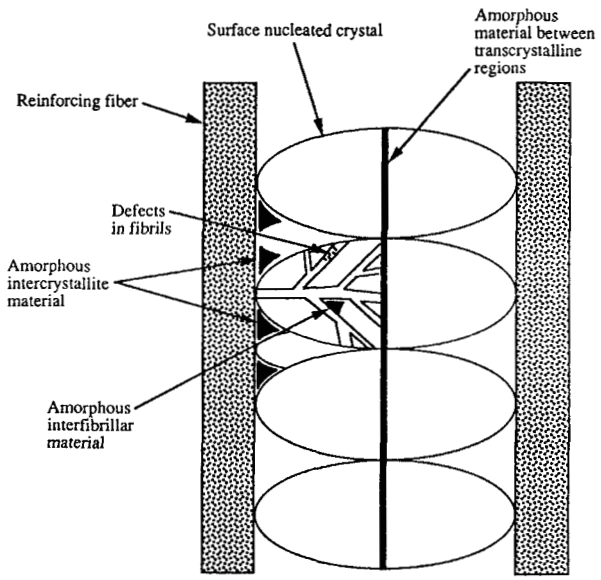

Figure 17 Schematic representation of transcrystalline structure.

Table XVI Values for the Arrhenius Temperature Dependence of the Rate Constants for the Primary and Secondary Crystallization Process as Determined from the Absolute Crystallinity as a Function of Time: Series Crystallinity Model

System	n_{c1}	E_{ac_1}	E_{gc_1}	$A_{K_{c1}}$	A_{gc_1}	n_{c2}	E_{ac_2}	E_{gc_2}	$A_{K_{c2}}$	A_{gc_2}
PPS (molded)	2.5	1.9	0.7	1.48×10^3	20	0.5	0.4	0.8	2.6	7
Unsized AS4 (54%)	2.2	1.5	0.7	0.50×10^3	20	0.3	0.4	1.2	3.7	80
Sized AS4 (64%)	2.3	1.8	0.8	3.33×10^3	30	0.5	0.4	0.8	3.2	10
Thornel (65%)	2.3	1.8	0.8	26.50×10^3	80	0.3	0.4	1.3	3.8	85
Unsized glass (67%)	2.1	1.4	0.7	0.08×10^3	10	0.4	0.4	0.9	1.9	5
Sized glass (65%)	2.3	1.5	0.7	0.16×10^3	10	0.4	0.4	1.1	3.1	16
Unsized Kevlar (58%)	2.3	2.1	0.9	62.30×10^3	120	0.4	0.4	1.1	4.4	42
Sized Kevlar (53%)	3.0	2.6	0.9	135.00×10^5	240	0.3	0.4	1.3	6.9	613

density of the fiber surface must be relatively high. As the surface-nucleated crystals grow, they are constrained by neighboring crystals to grow radially outward from the fiber surface, as schematically depicted in Figure 17. As the crystals grow outward, amorphous regions are trapped within and between the growing crystals in a manner similar to that which is visualized for normal spherulitic crystallization. However, since many more crystallites are nucleated, more amorphous material is trapped between crystallites than is observed for spherulitic systems, although the amorphous content trapped within the growing crystallites is presumed to be similar to that contained within a growing spherulitic crystal. As the crystallization process proceeds, the trapped amorphous regions undergo secondary crystallization, and crystallite perfection occurs in the surface-nucleated crystals.

The values for the overall frequency factors for the primary crystallization, A_{kc1}, shown in Table XVI, reflect the degree of interaction between the fiber surface and the crystallizing PPS molecules. The four highest values of the frequency factor occur in those systems that exhibit transcrystallinity, supporting the hypothesis that the higher fiber-surface interaction results in a transcrystalline morphology.

CONCLUSIONS

The classical Avrami model for polymer crystallization was found to provide a good description of the development of the volume fraction of material crystallized for those fiber-reinforced PPS composite systems that did not exhibit transcrystallinity. Nucleation was speculated to be athermal, while the growth habit of the polymer crystal was found to change from a predominance of three-dimensional spherulites in the unreinforced PPS to two-dimensional spherulites in the fiber-reinforced systems. Presumably, the presence of the reinforcing fibers constrains the growing polymer crystals to two-dimensional growth. The temperature dependence of the rate constants were found to follow an Arrhenius-type dependence on the degree of undercooling from the equilibrium crystallization temperature. The activation energies for each of the systems were similar and corresponded to a previously reported literature value for the activation energy of PPS molecular chain motion.

For those composite systems that exhibited a transcrystalline morphology, the Avrami model did not adequately describe the volume fraction of material crystallized. Instead, a combination of crystallization processes, either in series or in parallel, were used to model the kinetic data. While both models provided adequate descriptions of the crystallization process, some conceptual problems with these models make them unsatisfying. Yet both models provided insights into the factors that must be accounted for when analyzing the crystallization of reinforced polymer systems.

Finally, a model was proposed that accounts for the development of crystallinity rather than the volume fraction of material crystallized in these systems. The development of crystallinity was modeled using an Avrami-type equation. Two sequential processes were found to occur in all the systems investigated. These processes are presumed to be the development of crystallinity through primary crystallization and the subsequent enhancement of crystallinity due to secondary crystallization and/or crystallite perfection processes. The kinetics of the secondary crystallization process were independent of the presence or type of reinforcing fiber, whereas the kinetics of the primary process were found to depend on both the presence and type of

reinforcing fiber. Less crystallinity was observed to develop during the first process in the systems that exhibited transcrystalline morphologies as compared to those systems that exhibited spherulitic morphologies. Presumably, more amorphous regions are trapped in and between the growing surface nucleated crystals so that secondary crystallization processes become more important. In both types of crystallization processes, spherulitic and fiber-surface-nucleated, the crystallinity that is developed during the primary crystallization process is found to be moderately high.

The temperature dependence of the rate constants for each of the processes in the crystallinity model was found to follow an Arrhenius relationship. Activation energies were found to be similar to a reported literature value for the activation energy for molecular mobility of low molecular weight PPS. Finally, the frequency factors obtained from the crystallinity model were reflective of the interaction with the fiber surface and correlate with the presence of transcrystallinity.

The authors wish to acknowledge Professor S. Sundaresan of Princeton University for many helpful discussions.

REFERENCES

1. G. P. Desio and L. Rebenfeld, *J. Appl. Polym. Sci.*, to appear.
2. G. P. Desio and L. Rebenfeld, *J. Appl. Polym. Sci.*, **39,** 825–835 (1990).
3. M. Avrami, *J. Chem. Phys.*, **7,** 1103 (1939); **8,** 212 (1940); **9,** 177 (1941).
4. J. P. Jog and V. M. Nadkarni, *J. Appl. Polym. Sci.*, **30,** 997 (1985).
5. P. Cebe and S. Hong, *Polymer,* **27,** 1183 (1986).
6. C. N. Velisaris and J. C. Seferis, *Polym. Eng. Sci.*, **26**(22), 1574 (1986).
7. D. J. Blundell and B. N. Osborn, *SAMPE Q.*, **17**(1), 1 (1985).
8. P. Cebe, *Polym. Eng. Sci.*, **28**(18), 1192 (1988).
9. J. M. Kenny and A. Maffezzoli, *Polym. Eng. Sci.*, **31,** 607–614 (1991).
10. F. C. Perez-Cardenas, L. F. del Castillo, and R. Vera-Graziano, *J. Appl. Polym. Sci.*, **43,** 779–782 (1991).
11. A. J. Lovinger, D. D. Davis, and F. J. Padden, *Polymer,* **26,** 1595 (1985).
12. B. Wunderlich, *Macromolecular Physics: Volume 2. Crystal Nucleation, Growth, Annealing,* Academic Press, New York, 1976.
13. L. Rebenfeld, G. P. Desio, and J. C. Wu, *J. Appl. Polym. Sci.*, **42,** 801–805 (1991).

Received August 9, 1991
Accepted October 21, 1991